A ^{15}N NMR Mobility Study on the Dicalcium P43M Calbindin D_{9k} and Its Mono-La^{3+}-Substituted Form†

Ivano Bertini,‡ Carl J. Carrano,*,§ Claudio Luchinat,|| Mario Piccioli,‡ and Luisa Poggi‡

Magnetic Resonance Center (CERM) and Department of Chemistry, University of Florence, Sesto Fiorentino, Italy, Department of Chemistry and Biochemistry, Southwest Texas State University, San Marcos, Texas 78666, and Magnetic Resonance Center (CERM) and Department of Agricultural Biotechnology, University of Florence, Sesto Fiorentino, Italy

Received November 14, 2001; Revised Manuscript Received February 21, 2002

ABSTRACT: Calbindin D_{9k} is a dicalcium binding protein consisting of two helix−loop−helix EF-hand motifs joined together by a flexible linker region where one metal ion can bind to each of the two loops. A proline residue at position 43 in the linker region displays cis−trans isomerism in the wild-type (WT) protein. Such isomerism appeared to be removed by substituting the proline with a glycine or a methionine in the P43G or P43M mutant. We have extended the available mobility studies on the P43M mutant through amide ^{15}N R_1, R_2, and $R_{1\rho}$ measurements. This has revealed unexpected conformational equilibria on the millisecond time scale involving residues 38, 42−44, and 46 in the linker region and residues 18 and 19 in calcium binding site I with similar energy barriers. These data are discussed in comparison with those available for the WT, as well as the apo-, mono-, and disubstituted P43G mutant. Quantification of water−amide proton exchange rates using saturation transfer and qualitative application of ^{15}N-(CLEANEX-PM)-FHSQC shows the values are in agreement with high mobility for the above-mentioned residues. Cross correlation between N−H dipole−dipole relaxation and ^{15}N CSA relaxation indicates that some of these mobility differences may extend to the sub-nanosecond time scale. Similar data were also obtained for the derivative where the calcium ion in the C-terminal loop was replaced with lanthanum. The results presented here show that, contrary to expectations, there are significant differences in dynamics between the dicalcium state of P43G and P43M and that these differences are not confined to the flexible linker region containing the point mutation. They also demonstrate that substitution of a lanthanide ion for calcium, which is a common procedure, does not significantly alter the mobility of the native protein.

Calcium ion is an important second messenger in a wide variety of cellular functions (*1*). As a consequence, calcium-binding proteins make up an abundant and well-studied class of metalloproteins. One group of such proteins is characterized by a helix−loop−helix structure known as an EF-hand. Often two or more EF-hand motifs are connected via a flexible linker segment that may lead to cooperative interactions between the Ca^{2+} binding centers (*2*). It is generally believed that those EF-hand proteins with a regulatory role are activated for interaction with other cellular proteins by large conformational changes associated with calcium binding, while those associated with ion buffering or transport undergo much smaller structural modifications (*3*−*5*). A particularly well-studied example of an EF-hand is the small (8.5 kDa) calcium binding protein calbindin D_{9k}.

Calbindin D_{9k} (Cb hereafter) is a dicalcium binding protein consisting of four helices and two EF-hands joined together by a flexible linker region with one metal ion bound to each of the two loops. The protein is implicated in intracellular Ca^{2+} transport. Structures of the apo (*6*), the dicalcium (CaCaCb) (*6*), monolanthanide-substituted (CaLnCb) (*7*), monocadmium (CdCb) (*8*), and dimagnesium (MgMgCb) (*8*) complexes have all been determined by either NMR[1] or X-ray diffraction techniques. The NMR structure of the CaLnCb derivative is shown in Figure 1 (PDB entry 1KSM) (*7*). These structures have revealed that as expected only very minor changes occur in the N-terminal EF-hand upon Ca^{2+} binding, while somewhat larger changes accompany binding to the C-terminal site.

† This research has been financially supported by the RTD projects ("FIND Structure" Contract QLG2-CT-1999-01003) and ("Transient NMR" Contract HPRI-CT-1999-50006). Financial support for C.J.C.'s stay in Florence was provided by the Fogarty International Center of the NIH through Grant F06-TW02239-01, which is gratefully acknowledged.

* To whom correspondence should be addressed. E-mail: cc05@swt.edu. Fax: (512) 245-2374. Phone: (512) 245-3117.

‡ Magnetic Resonance Center and Department of Chemistry, University of Florence.

§ Southwest Texas State University.

|| Magnetic Resonance Center and Department of Agricultural Biotechnology, University of Florence.

[1] Abbreviations: NMR, nuclear magnetic resonance; CSA, chemical shift anisotropy; HSQC, heteronuclear single-quantum correlation; FHSQC, fast heteronuclear single-quantum correlation; CLEANEX-PM, phase-modulated clean chemical exchange; NOE, nuclear Overhauser effect; WT, wild type; P43G, calbindin D_{9k} mutant with the Pro43 → Gly substitution; P43M, calbindin D_{9k} mutant with the Pro43 → Met substitution; M_1M_2Cb, calbindin D_{9k} with metal ion M_1 in site I and M_2 in site II. Amino acids are denoted by their standard one- and three-letter codes

10.1021/bi015945n CCC: $22.00
Published on Web 03/30/2002

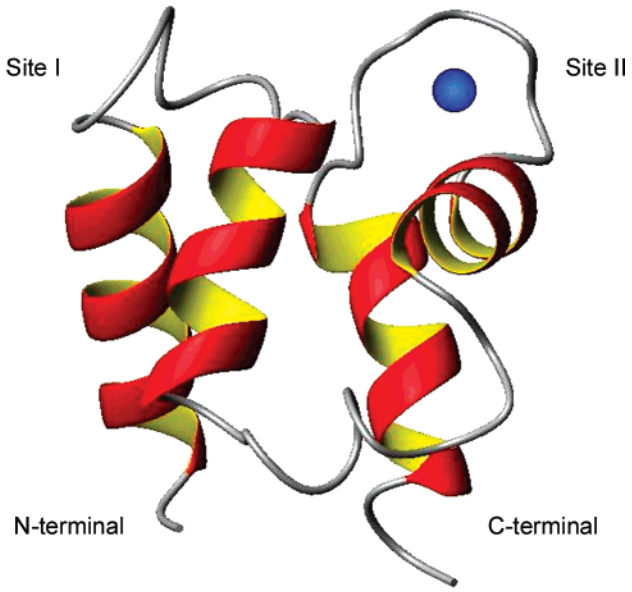

FIGURE 1: Structure of CaLnCb P43M (PDB entry 1KSM).

In contrast to the small structural changes accompanying Ca^{2+} binding to calbindin, ^{15}N relaxation and amide proton exchange studies have revealed dramatic effects on the dynamical properties of the protein on a wide variety of time scales (*8*, *10*−*12*). Since wild-type calbindin displays a cis−trans isomerization about the Gly42−Pro43 amide bond that results in two distinct sets of NMR resonances (*13*), most such studies have utilized the recombinant P43G and P43M mutants. The available evidence suggests that in solution at pH 6.0 the structural changes induced by these substitutions are very minor and localized around the site of the mutation in the flexible linker region (*13*). Nonetheless, it has recently been reported that under crystallization conditions (pH ~5.0) the P43M mutant dimerizes in the solid state via so-called EF-hand subdomain swapping (*14*). The formation of a hydrophobic cluster in the region linking the EF-hands appears to promote the formation of the three-dimensional (3D) domain-swapped dimer.

Lanthanide ions have long been used as probes for the spectroscopically silent Ca^{2+} ion in many calcium ion-binding proteins (*15*−*17*). These studies have utilized both the luminescent and magnetic properties of the lanthanides to obtain information about the structure and function of the native Ca^{2+} systems. It is clear that despite the differences in charge between the lanthanide and calcium ions, replacement of the latter by the former causes only very minor structural rearrangements (*18*), justifying their use as structural probes. However, little or no data are available concerning how such substitutions affect the dynamic properties of the protein. Since lanthanide ion probes have been used to study the NMR characteristics of calbindin (*7*, *16*, *19*), we have been prompted to compare the protein dynamics of this system to determine if the substitution of Ca^{2+} with La^{3+}, with its higher charge, had any significant effects on protein mobility.

Protein dynamics occur on a wide variety of time scales and have important implications with respect to the functions such as enzyme activity and ligand binding (*20*, *21*). Nuclear spin relaxation methods provide data on both the fast (picosecond to nanosecond) and slow (microsecond to millisecond) internal motions, while magnetization transfer is sensitive to protein movements on the millisecond to second time scale. Since many biochemically significant properties such as protein local stability, redox potentials, and protein−protein interactions are all related to motions on the microsecond to millisecond time scale and the fact that both the very fast and very slow dynamics on calbindin D_{9k} have already been studied by others (*10*, *12*, *22*), we have chosen to concentrate our efforts on this time regime. For the sake of completeness and to facilitate comparisons, we have also looked at fast and slow protein mobility via cross correlation and saturation transfer experiments, respectively. In this report, we compare these dynamics for the CaCaCb P43M with those of the C-terminal La^{3+}-substituted protein (CaLaCb) and with those already reported for the CaCaCb P43G mutant.

MATERIALS AND METHODS

Sample Preparation. Protein expression (*23*) and purification (*24*) of both the Ca^{2+} and the apo form of the bovine Pro43 → Met (P43M) mutant (*25*, *26*) of calbindin D_{9k} were performed as reported. The expression system was a generous gift of S. Forsén. Uniformly ^{15}N-labeled overexpressed P43M was obtained from M9 minimal medium containing $(^{15}NH_4)_2SO_4$ as the sole nitrogen source. The site II lanthanum substitution procedure is described elsewhere (*19*). The pH was adjusted to 6.0 by means of 0.1 M NaOH or 0.1 M HCl. The samples were kept at 4 °C between measurements.

NMR Experiments. All NMR experiments for determination of ^{15}N and ^{1}H relaxation rates were recorded at 300 K, except when otherwise specified, on 2.0 mM samples on Bruker Avance 400 and 700 spectrometers.

^{15}N $R_2(1/\tau_{cp})$ relaxation rates at 9.4 and 16.4 T were measured using the relaxation-compensated Carr−Purcell−Meiboom−Gill (CPMG hereafter) pulse sequences previously reported in the literature (*27*). For both B_0 fields and both CaCaCb and CaLaCb derivatives, data were collected for τ_{cp} values of 1.0, 1.5, 2.0, 4.0, 6.6, 10.8, 21.5, and 64.5 ms. Spectra were acquired using 128 × 2048 complex points and spectral widths of 30.0 and 13.0 ppm in the t_1 and t_2 dimensions, respectively. The ^{1}H carrier frequency was set coincident with the water resonance; the ^{15}N carrier frequency was set to 115.5 ppm. The recycle delay was 3 s. A total of 16 transients were recorded for each complex point. The free induction decays were processed in F_2 by apodizing with a cosine bell window function, zero-filling once, and Fourier transforming. The resulting spectra were phase and baseline-corrected. The F_1 interferograms were apodized with a cosine bell window function, zero-filled once, Fourier transformed, and phase corrected.

Off-resonance rotating frame relaxation rates, $R_{1\rho}^{OFF}$, were measured as a function of the effective spin-lock power at 9.4 T using a previously reported sequence (*28*). For both CaCaCb and CaLaCb, $R_{1\rho}^{OFF}$ measurements were recorded at 10 different effective spin-lock power values (the corresponding tilt angles are given in parentheses): 5.19 (35°), 4.64 (35°), 4.11 (35°), 3.66 (35°), 3.28 (35°), 2.98 (35°), 2.66 (50°), 2.36 (50°), 2.10 (50°), and 1.88 kHz (50°). The effective spin-lock power was varied either by varying the offset between the frequency at which the spin lock was applied and the frequency corresponding to the center of the

^{15}N window (held constant) or by changing the applied B_1 field strength. For each $R_{1\rho}^{OFF}$ measurement, data were collected for a spin-lock period of 10, 20, 36, 60, 86, 100, 150, and 200 ms. A trapezoid-shaped spin-lock adiabatic pulse with a 2 ms ramp in amplitude was always applied. The conditions of acquisition that were used were the same of those for the $R_2(1/\tau_{cp})$ measurements.

Measurements of the cross correlation between ^{15}N−^{1}H dipolar interaction and ^{15}N CSA were carried out at 16.4 T using a previously reported sequence (*29*). Durations for the dephasing delay, 2Δ, were 46.7, 68, and 132 ms. The conditions of acquisition that were used were the same as those for the $R_2(1/\tau_{cp})$ measurements.

^{15}N R_1 relaxation rates were measured at 9.4 T for both CaCaCb and CaLaCb using an already reported sequence modified to remove cross correlation effects during the relaxation delay (*30*). The recycle delay was 1.8 s, and water flip-back was used to suppress the strong solvent signal. Ten experiments were carried out, with recovery delays of 10, 70, 150, 250, 380, 540, 740, 1000, 1350, and 3000 ms. The experimental conditions were the same as for the measurement of ^{15}N R_2 relaxation rates.

Amide proton exchange rates were initially measured using NMR saturation transfer experiments (*31*, *32*). In these experiments, a ^{15}N HSQC correlation spectrum acquired with no presaturation was compared with one with 3.0 s of presaturation. Fast amide proton exchange rates were also measured using ^{15}N-(CLEANEX-PM)-FHSQC experiments (*33*, *34*) with a mixing time of 100 ms.

All NMR data were processed with the Bruker XWIN-NMR software package.

RESULTS

Protein motions on the microsecond to millisecond time scales are normally due to chemical or conformational kinetic phenomena (*20*, *21*). Such exchange processes contribute to the transverse relaxation rate and can be studied by ^{15}N NMR relaxation measurements for the amide backbone resonances using CPMG (laboratory frame) or $R_{1\rho}$ (rotating frame) experiments. These exchange processes can then be quantified, typically by measuring R_2 as a function of $1/\tau_{cp}$ in the CPMG experiments or $R_{1\rho}$ as a function of the effective spin-lock field in the rotating frame experiments. In the study presented here, we have utilized both methods.

Laboratory Frame Experiments. For CaCaCb, R_1 values (Table 1) were measured at 400 MHz and 300 K and were as expected quite uniform. The average value is 3.01 ± 0.26 s^{-1} for all data which reduces to 3.08 ± 0.10 s^{-1} when values more than SD from the average were excluded. These latter values corresponded to residues near the termini and in the flexible linker region (residues 40−45). ^{15}N $R_2(1/\tau_{cp})$ values were measured at several values of τ_{cp} with the data for a τ_{cp} of 1 ms being representative (Table 1). The R_2/R_1 ratio is a useful diagnostic parameter for the preliminary evaluation of relaxation data (*35*, *36*). Values of R_2/R_1 substantially greater than the mean are indicative of the presence of chemical exchange phenomena which increase R_2, while values below the mean are the result of fast internal motions contributing to the relaxation. The results for P43M are shown in Table 1 and Figure 2.

Table 1: ^{15}N Relaxation Parameters for CaCa P43M Calbindin D_{9k} at 300 K

residue	^{15}N R_1 (s^{-1})	^{15}N R_2 (s^{-1})	R_2/R_1	residue	^{15}N R_1 (s^{-1})	^{15}N R_2 (s^{-1})	R_2/R_1
1	–	–	–	39	3.024	7.84	2.59
2	2.726	7.827	2.87	40	2.842	7.37	2.59
3	–	–	–	41	2.653	7.56	2.85
4	3.042	8.267	2.72	42	2.429	8.73	3.59
5	2.921	8.127	2.78	43	2.892	16.71	5.78
6	3.041	8.85	2.91	44	2.523	12.25	4.86
7	3.169	8.94	2.82	45	2.702	7.26	2.69
8	3.128	8.32	2.66	46	3.207	10.96	3.42
9	3.154	8.99	2.85	47	3.017	8.00	2.65
10	3.114	8.82	2.83	48	3.056	8.51	2.78
11	3.158	9.23	2.92	49	3.073	8.60	2.80
12	3.107	8.47	2.73	50	3.113	8.86	2.85
13	3.023	8.86	2.93	51	3.118	8.55	2.74
14	3.169	8.74	2.76	52	3.056	8.02	2.62
15	3.098	8.11	2.62	53	2.728	7.04	2.58
16	2.923	7.71	2.64	54	3.073	8.50	2.77
17	3.035	7.62	2.51	55	2.898	8.20	2.83
18	3.274	11.42	3.49	56	3.095	7.65	2.47
19	2.959	13.53	4.57	57	3.03	7.90	2.61
20	–	–	–	58	3.047	7.52	2.47
21	3.057	7.99	2.61	59	3.143	8.16	2.60
22	3.063	7.75	2.53	60	3.102	7.61	2.45
23	3.144	9.31	2.96	61	3.106	9.07	2.92
24	3.161	9.59	3.03	62	3.105	9.55	3.08
25	3.155	9.37	2.97	63	3.126	9.34	2.99
26	3.053	8.38	2.74	64	3.015	8.30	2.75
27	3.154	9.37	2.97	65	3.166	9.14	2.89
28	3.169	9.33	2.94	66	3.166	9.35	2.95
29	3.177	9.18	2.89	67	3.135	8.53	2.72
30	3.113	9.03	2.90	68	3.134	8.60	2.74
31	3.18	9.36	2.94	69	3.107	8.70	2.80
32	3.212	9.48	2.95	70	2.958	8.45	2.86
33	3.162	8.70	2.75	71	3.008	8.23	2.74
34	3.124	8.71	2.79	72	2.829	7.76	2.74
35	3.118	9.15	2.93	73	2.736	7.39	2.70
36	2.966	8.21	2.77	74	2.683	7.43	2.77
37	–	–	–	75	1.347	3.41	2.53
38	3.206	11.66	3.64				

The mean R_2/R_1 ratio also allows for an estimate of the τ_m of the protein (*37*). The average value of R_2/R_1 is 2.91 ± 0.52 which decreases to 2.77 ± 0.15 when residues (Gly18, Asp19, Ser38, Gly42, Met43, Ser44, and Leu46) which deviated more than SD from the average were excluded. This indicates that exchange phenomena were active for these seven residues. Surprisingly, for the analogous CaCaCb P43G, no residues showed evidence for significant exchange broadening (*12*). Thus, in contrast to expectations based on the small and extremely localized chemical shift differences and structures between the two mutant proteins, their dynamical properties appear to be significantly different. In addition, these dynamical changes are not restricted entirely to the site of the mutation. Similar experiments were performed on a sample of CaLaCb. The results (Supporting Information) show that the La^{3+}-substituted protein has dynamic properties very similar to those of the Ca^{2+} analogue. A notable difference is the increase in the exchange contributions to R_2 for residues Gly18 and Asp19 located in loop I and for residue Gly42 in the linker region. Smaller changes in the R_2/R_1 ratio are also found for Met43 and Ser44. However, these changes are marginal with respect to the differences between the P43M and P43G variants.

Attempts to obtain dispersion curves for a quantitative determination of the R_{ex} contribution to R_2 were thwarted by a lack of observable dispersion in plots of R_2 versus $1/\tau_{cp}$

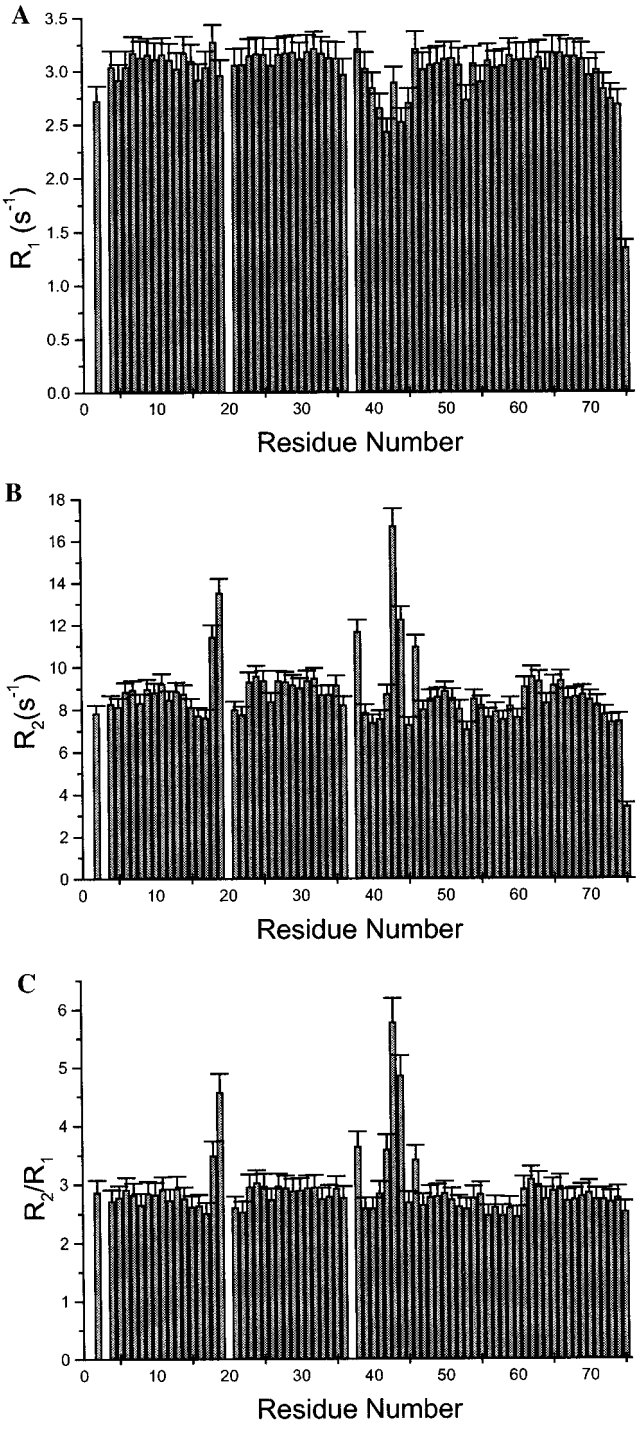

FIGURE 2: Bar graphs of ^{15}N amide relaxation rates of the P43M CaCaCb derivative, collected at 400 MHz and 300 K. R_1 (A), R_2 (B), and the R_2/R_1 ratio (C) are shown.

over the experimentally accessible range for either the CaCaCb or CaLaCb proteins. The lack of observable dispersion suggests that k_{ex} must be >1000 s^{-1} (*27*).

$R_{1\rho}$ Experiments. In an attempt to quantify the exchange contribution to R_2, we also undertook $R_{1\rho}$ experiments which allowed us to access somewhat faster rate constants than the CPMG approach (*28*, *38*). We performed both "on-resonance" and "off-resonance" $R_{1\rho}$ experiments. $R_{1\rho}$ is related to R_2 by eq 1 (*28*):

$$R_{1\rho}(\theta,\omega) = \cos^2\theta \times R_1 + \sin^2\theta \times R_2 + R_{ex}(\theta,\omega) \quad (1)$$

Table 2: Values of R_{ex} for CaCaCb P43M at 300 K

residue	R_{ex} (s^{-1})	residue	R_{ex} (s^{-1})
18	3.13	43	8.42
19	5.24	44	3.96
38	3.37	46	2.67
42	3.44		

where R_1 is the longitudinal relaxation rate, R_2 the transverse self-relaxation rate, and R_{ex} the relaxation rate associated with the exchange process. When off-resonance effects are neglected (which may become significant for wide sweep widths), $\theta = 90°$ for the on-resonance experiment. Hence, $R_{1\rho}$ measurements provide the same information as R_2 measurements. In the off-resonance experiment, the rotating frame is tipped by an angle θ with respect to the laboratory frame, and in this case, R_2 is calculated from eq 1 using two different θ values of 35° and 50°. Unfortunately, these data show no dispersion in R_2 as a function of ω_{eff} and thus do not provide any new information relative to the more easily performed CPMG experiments and do not allow a more quantitative determination of R_{ex}.

Temperature Dependence of R_2. Since no dispersion in R_2 values as a function of $1/\tau_{cp}$ was noted in the CPMG experiments at 300 K, we obtained data at 283, 290, 295, and 305 K since the temperature dependence of R_{ex} can sometimes be used to determine the time scale of chemical exchange (*39*, *40*). Thus, if $k_{ex} > 3.2 \times 10^3$ s^{-1} for a τ_{cp} of 1 ms, then increasing T decreases R_{ex}; conversely, if $k_{ex} < 3.2 \times 10^3$ s^{-1}, then increasing T increases R_{ex} (*41*). In the case presented here, R_{ex} values were approximated on the basis of the equation $R_{ex} = R_2(n) - R_2$(mean). This approximation will severely underestimate R_{ex} for those residues whose intrinsic R_2 values are below the mean as a result of fast internal motions contributing to the relaxation. This is likely to be the case for residues 38, 42−44, and 46 that lie in the linker region where such fast motions are known to occur. Thus, values of R_{ex} obtained by this approximation can be considered only as lower limits. The values of R_{ex} estimated from the 300 K data are given in Table 2. In this case, the data show that the exchange contribution to R_2 for residues Gly18, Asp19, Ser38, Gly42, Met43, Ser44, and Leu46 decreases between 305 and 283 K. Thus, k_{ex} must be $<3.2 \times 10^3$ s^{-1}. Plots of ln R_{ex} versus $1/T$ were linear and followed the Arrhenius equation (Figure 3), allowing calculation of the apparent activation energies from the slope of such plots. The activation energies for the kinetic processes occurring at residues in the flexible linker region and those in the first Ca^{2+} binding loop are essentially the same (30 ± 10 kcal/mol), lending support to the notion of a simple two-site exchange process accounting for the kinetic effects observed at all seven residues.

Unfortunately, temperature changes also perturb the site populations (assuming a simple two-site exchange model) through the Boltzmann equation and can affect $\Delta\omega$ through temperature-dependent conformational changes, potentially complicating any interpretation of the temperature dependence of R_{ex}. Therefore, Palmer et al. (*27*) have suggested the use of the static field dependence of R_{ex} for determining the NMR chemical shift time scale for an exchange process

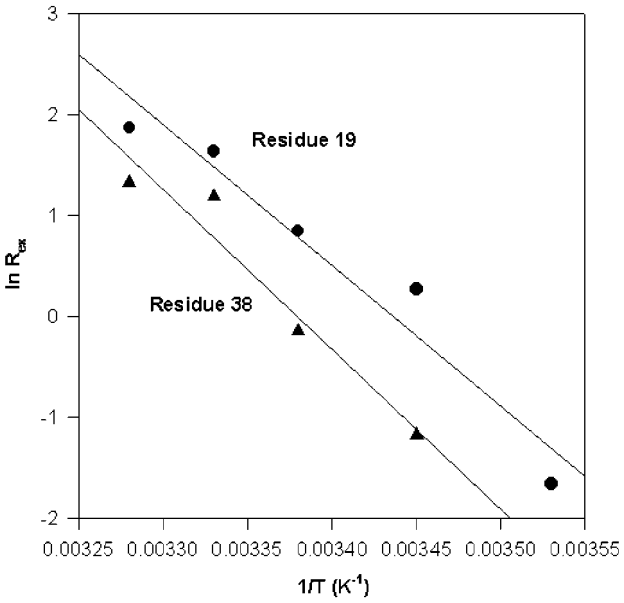

FIGURE 3: Arrhenius plot of the observed exchange rates for selected residues of CaCaCb P43M.

through a scaling factor, α, defined by

$$\alpha = \frac{\mathrm{d}(\ln R_{ex})}{\mathrm{d}(\ln \Delta\omega)} \tag{2}$$

For slow exchange ($k_{ex}/\Delta\omega < 1$), $0 \leq \alpha < 1$; for intermediate exchange ($k_{ex}/\Delta\omega = 1$), $\alpha = 1$, and for fast exchange ($k_{ex}/\Delta\omega > 1$), $1 < \alpha \leq 2$. Using data at both 400 and 700 MHz, R_{ex} values for all seven residues appear to be essentially independent of the static magnetic field, i.e., $\alpha \approx 0$, demonstrating that the system is in slow exchange on the NMR chemical shift time scale.

Fast Protein Dynamics via Cross Correlation Experiments. Since the slow protein dynamics of P43M were significantly different from those of P43G, we attempted to determine if these differences extended to the fast protein dynamic regime. These dynamics are usually evaluated in a quantitative way via the so-called model free approach (*42*−*44*). However, it has been pointed out by Bax et al. (*29*) that simpler relaxation interference experiments between ^{1}H−^{15}N dipole−dipole coupling and ^{15}N chemical shift anisotropy can give equivalent information concerning the order parameters (S^2) within a precision of 5−10%. We have performed such cross correlation experiments on both CaCaCb and CaLaCb. The results (Figure 4) show that while both P43M mutant proteins behave in general, similar to the well-studied CaCaCb P43G mutant on the picosecond to nanosecond time scale, some differences can be found. In particular, residues 17−19, 53, and 61 appear to be more flexible in the P43M mutant than in the P43G mutant, while residue 43 seems to be more rigid.

Amide Proton Exchange Rates. Conformational exchange phenomena that open parts of the protein backbone and expose it to bulk solvent are expected to give rise to relatively fast amide proton exchange kinetics. The rates of such amide proton exchange with solvent in the range of 0.1−90 s^{-1} are easily measured via NMR saturation transfer experiments (*31*, *32*). The process is described by eq 3, when the

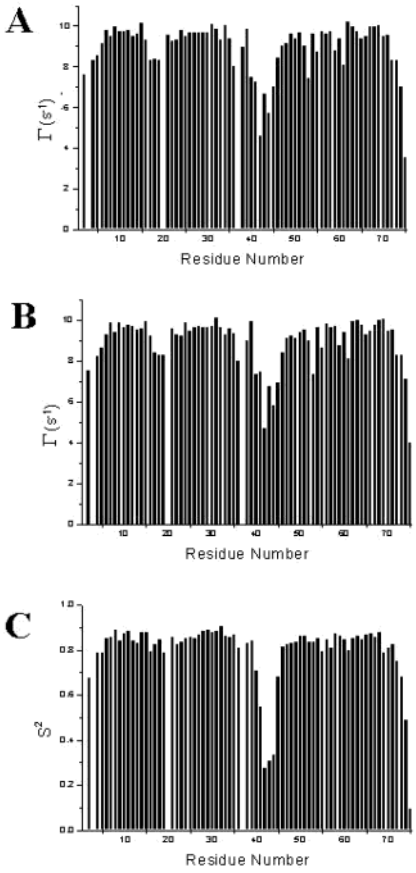

FIGURE 4: Bar graphs of ^{1}H−^{15}N to ^{15}N CSA cross correlation rate (Γ) observed for CaCaCb (A) and CaLaCb (B) at 700 MHz and 300 K. The results are very similar to previously reported S^2 values; see ref *12* (C).

irradiation time t is long compared with amide proton T_1:

$$\frac{I_t}{I_0} = \frac{1}{1 + k_{ex}T_1} \tag{3}$$

Thus, a comparison of the intensities of the peaks in the ^{15}N HSQC correlation spectrum acquired with no presaturation and that with 3.0 s of presaturation allows estimates of k_{ex}^{chem} to be made. A plot of k_{ex}^{chem} versus residue number is shown graphically in Figure 5. It is evident that as expected the fastest amide proton exchange in general takes place in the three loop regions. Peak values of k_{ex}^{chem} are observed for residues 18, 19, 38, and 42−44, i.e., those residues that show evidence of conformational mobility on the microsecond to millisecond time scale. However, interpretation of high apparent exchange rates via saturation transfer experiments can be complicated by the need to account for exchange-relayed NOEs, i.e., intramolecular effects due to fast exchanging protein protons. The use of the ^{15}N-(CLEANEX-PM)-FHSQC approach (Figure 6) eliminates this ambiguity and confirms that the aforementioned residues do indeed experience high amide proton exchange rates. It therefore appears that the conformational exchange evident on the microsecond to millisecond time scale is also reflected in the longer time scale of the amide hydrogen exchange experiments. No significant differences between P43M CaCaCb and CaLaCb were evident (data not shown), in keeping with the similarities in the microsecond to millisecond dynamics of the two proteins.

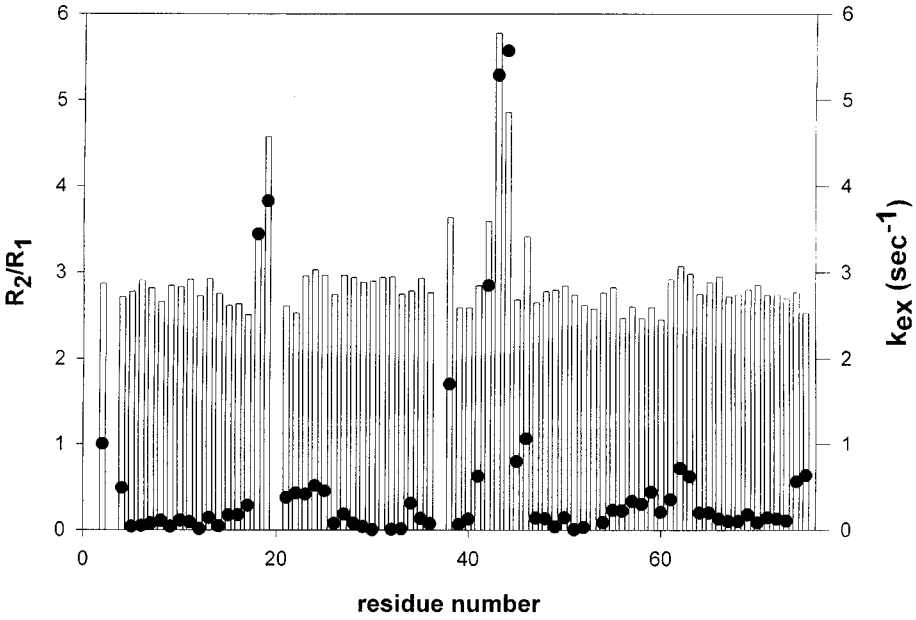

FIGURE 5: Plot of amide proton exchange rates as determined by saturation transfer methods superimposed on a bar graph of R_2/R_1.

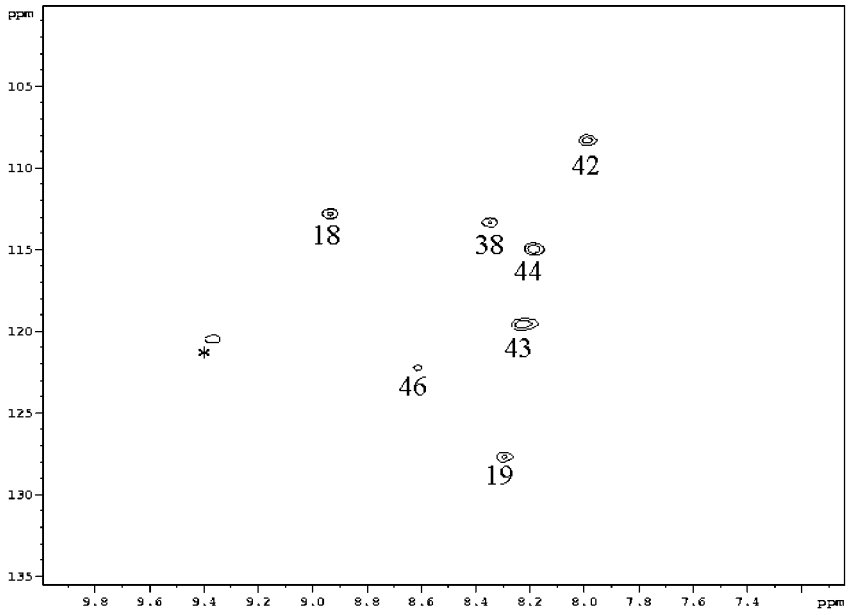

FIGURE 6: Data from a ^{15}N-(CLEANEX-PM)-FHSQC experiment collected on CaCaCb at 400 MHz and 300 K. Backbone peaks are labeled according to amino acid number. The peak labeled with an asterisk is unassigned.

DISCUSSION

Both the structure and dynamics on a wide variety of time scales of the wild type and the P43G mutant of calbindin D_{9k} have been extensively studied (*10*, *12*, *22*, *32*). These studies have included the apo, CaCaCb, and various mono-substituted metal derivatives such as Cd^{2+}. Very little work has been performed on the dynamics of the P43M mutant, despite its widespread use. The previously available evidence and "chemical intuition" both suggested that differences between the two proteins were minor. However, the results presented here show that, contrary to expectations, there are significant differences in dynamics on the microsecond to millisecond time scale between the dicalcium state of P43G and P43M and that these differences are not confined to the flexible linker region containing the point mutation. While in CaCaCb P43G no residues showed evidence of an exchange contribution to R_2, seven residues (Gly18, Asp19, Ser38, Gly42, Met43, Ser44, and Leu46) show such exchange in P43M. In this regard, CaCaCb P43M more resembles the apo and CdCb P43G variants than that of the corresponding dicalcium derivative (*32*). CdCb P43G shows a number of residues in loop I (which is unoccupied), including Gly18 and Asp19, with significant exchange broadening, as does CaCaCb P43M. The kinetic process observed in CdCb P43G, which has a rate constant estimated to be >2000 s^{-1}, has been attributed to exchange between two distinct conformers rather than chemical exchange between CdCb and some small population of CdCdCb. Similar conclusions were reached for the apo form where exchange with a small amount of CaCaCb was also consid-

ered an unlikely explanation for the observed kinetic process. The same conclusion, namely, that the kinetic process represents an exchange between two conformers rather than exchange between CaCaCb and some small population of either CaCb, apo-Cb, or both, can be reached for the CaCaCb P43M mutant since adding Ca^{2+} in 5−500% molar equiv excess has no effect on the microsecond to millisecond dynamics. Although rate constants for the kinetic processes observed in CaCaCb P43M cannot be determined directly, the fact that there is no dependence of R_2 as a function of $1/\tau_{cp}$ indicates that k_{ex} must be >1000 s^{-1}, while the temperature dependence of R_{ex} suggests a rate constant of <3200 s^{-1}.

What then is the nature of the observed kinetic process(es)? Wild-type CaCaCb is known to be in very slow exchange between two distinct conformers due to cis−trans isomerization about the Gly42−Pro43 bond (*13*), but such an isomerization is unlikely for amino acid residues other than proline. However, hydrophobic side chain interactions are crucial in the stabilization of the calbindin D_{9k} global fold; its four-helix bundle domain is a fold in which the amphipathic helices pack against one another to form a hydrophobic core of nonpolar residues from all four helices. The polar residues on the outer sides of the helices decorate the surface of the domain and solubilize it. Hakansson et al. (*14*) have studied an EF-hand domain swapping which occurs in the P43M mutant of calbindin. The Pro43 → Met substitution seems to be the major reason for the swapping, since the Met43 side chains of two monomers stabilize the dimer by packing into the hydrophobic core. In this way, two hydrophobic residues completely exposed in the monomer are protected from the solvent in the dimer. While actual dimer formation is found in the solid state only when crystallized at low pH (∼5.0) and very high protein concentrations, and NMR studies of P43M at pH 6.0 in solution do not reveal dimers (*7*, *18*), a weak interaction between the methionine side chain methyl and the hydrophobic core is quite possible. In this work, fast protein dynamics indicate that Met43 has a more restricted motion than its neighbors (Figure 4), suggesting that its side chain may be directed toward the protein core. This "redirection" of the Met43 side chain can (i) be responsible for the conformational exchange highlighted by the millisecond dynamics and (ii) affect the mobility of other residues belonging to the hydrophobic core of the protein. In particular, as shown in the fast dynamics results summarized in Figure 4, residues 17−19, 53, and 61 appear to be more flexible in the P43M mutant than in the P43G mutant. All these residues are involved in the hydrophobic core of the protein. In this regard, the P43M mutant is a better dynamic model for the WT protein. Thus, while the overall Ca^{2+} binding constants for WT, P43M, and P43G are essentially identical ($\sim 10^{16}$ M^{-2} s^{-2}), the dissociation off rates among the three vary. The Ca^{2+} dissociation off rate for the WT is 5.3 s^{-1}, similar to that of the P43M mutant (7.3 s^{-1}), while that of the P43G mutant is significantly higher at 60 s^{-1} (*13*, *45*). This trend mirrors the apparent conformer exchange rates (very slow for the WT, intermediate for P43M, and very fast for P43G). It therefore appears that the changes in the rate of exchange between conformers induced by point mutations could have significant biochemical consequences in this and other systems.

Conclusions. With this work, we have demonstrated that major changes in protein dynamics on the millisecond time scale accompany the P43G to P43M point mutation in calbindin D_{9k}. The linker region in the P43M mutant of the protein is affected by a conformational exchange phenomenon that is believed to be due to an interaction of the Met43 side chain methyl with the protein hydrophobic core. Moreover, these changes in the protein dynamics are not limited to the region near the mutation site but extend to the first Ca^{2+} binding loop, leaving unaffected the second Ca^{2+} binding loop. These results demonstrate that point mutations even far from the active site may have unexpected consequences that should be taken into account while designing a mutant and preparing to study its structural and dynamics properties.

On the other hand, this work confirms that lanthanides are good structural and dynamic probes for Ca^{2+} binding since both fast and slow mobility of Cb are unaffected by the selective replacement of calcium with a lanthanum ion in site II.

ACKNOWLEDGMENT

Dr. Renato Barbieri and Dr. Michael Akke are acknowledged for useful discussions. We thank two reviewers for their helpful and insightful comments.

SUPPORTING INFORMATION AVAILABLE

^{15}N relaxation parameters for CaLa P43M Calbindin D_{9k} at 300 K. This material is available free of charge via the Internet at http://pubs.acs.org.

REFERENCES

1. Heizmann, C. W., and Hunziker, W. (1991) *Trends Biochem. Sci. 16*, 98−103.
2. Linse, S., Brodin, P., Drakenberg, T., Thulin, E., and Sellers, P. (1987) *Biochemistry 26*, 6723−6735.
3. McPhalen, C. A., Strynadka, N. C. J., and James, M. N. G. (1991) *Adv. Protein Chem. 42*, 77−144.
4. Strynadka, N. C. J., and James, M. N. G. (1989) *Annu. Rev. Biochem. 58*, 951−998.
5. Ikura, M. (1996) *Trends Biochem. Sci. 21*, 14−17.
6. Svensson, L. A., Thulin, E., and Forsén, S. (1992) *J. Mol. Biol. 223*, 601−606.
7. Bertini, I., Donaire, A., Jimenez, B., Luchinat, C., Parigi, G., Piccioli, M., and Poggi, L. (2001) *J. Biomol. NMR 21*, 85−98.
8. Kordel, J., Skelton, N. J., and Chazin, W. J. (1993) *J. Mol. Biol. 231*, 711−734.
9. Berman, H. M., Westbrook, J., Feng, Z., Gilliland, G., Bhat, T. N., Weissig, H., Shindyalov, I. N., and Bourne, P. E. (2000) *Nucleic Acids Res. 28*, 235−242.
10. Akke, M., Skelton, N. J., Kördel, J., Palmer, A. G., III, and Chazin, W. J. (1993) *Biochemistry 32*, 9832−9844.
11. Akke, M., Forsén, S., and Chazin, W. J. (1991) *J. Mol. Biol. 220*, 173−189.
12. Kordel, J., Skelton, N. J., Akke, M., Palmer, A. G., III, and Chazin, W. J. (1992) *Biochemistry 31*, 4856−4866.
13. Kördel, J., Forsén, S., Drakenberg, T., and Chazin, W. J. (1990) *Biochemistry 29*, 4400−4409.
14. Hakansson, K., Svensson, A., Fast, J., and Linse, S. (2001) *Protein Sci. 10*, 927−933.
15. Banci, L., Bertini, I., and Luchinat, C. (1985) in *Rare Earths Spectroscopy* (Trebiatowska, B. J., Legendziewicz, J., and Strek, W., Eds.) pp 80−99, World Scientific, Singapore.
16. Bertini, I., Janik, M. B. L., Lee, Y.-M., Luchinat, C., and Rosato, A. (2001) *J. Am. Chem. Soc. 123*, 4181−4188.

17. Bentrop, D., Bertini, I., Cremonini, M. A., Forsén, S., Luchinat, C., and Malmendal, A. (1997) *Biochemistry 36*, 11605−11618.
18. Bertini, I., Lee, Y.-M., Luchinat, C., Piccioli, M., and Poggi, L. (2001) *ChemBioChem 2*, 550−558.
19. Allegrozzi, M., Bertini, I., Janik, M. B. L., Lee, Y.-M., Liu, G., and Luchinat, C. (2000) *J. Am. Chem. Soc. 122*, 4154−4161.
20. Ishima, R., and Torchia, D. A. (2000) *Nat. Struct. Biol. 7*, 740−743.
21. Kay, L. E. (1998) *Nat. Struct. Biol. 5*, 513−517.
22. Akke, M., Brüschweiler, R., and Palmer, A. G., III (1993) *J. Am. Chem. Soc. 115*, 9832−9833.
23. Brodin, P., Grundstrom, T., Hofmann, T., Drakenberg, T., Thulin, E., and Forsén, S. (1986) *Biochemistry 25*, 5371−5377.
24. Johansson, C., Brodin, P., Grundstrom, T., Thulin, E., Forsén, S., and Drakenberg, T. (1990) *Eur. J. Biochem. 187*, 455−460.
25. Malmendal, A., Carlström, G., Hambraeus, C., Drakenberg, T., Forsén, S., and Akke, M. (1998) *Biochemistry 37*, 2586−2595.
26. Chazin, W. J., Kördel, J., Drakenberg, T., Thulin, E., Brodin, P., Grundstrom, T., and Forsén, S. (1989) *Proc. Natl. Acad. Sci. U.S.A. 86*, 2195−2198.
27. Millet, O., Loria, J. P., Kroenke, C. D., Pons, M., and Palmer, A. G., III (2000) *J. Am. Chem. Soc. 122*, 2867−2877.
28. Zinn-Justin, S., Berthault, P., Guenneugues, M., and Desvaux, H. (1997) *J. Biomol. NMR 10*, 363−372.
29. Tjandra, N., Szabo, A., and Bax, A. (1996) *J. Am. Chem. Soc. 118*, 6886−6891.
30. Kay, L. E., Nicholson, L. K., Delaglio, F., Bax, A., and Torchia, D. A. (1992) *J. Magn. Reson. 97*, 359−375.
31. Hoffmann, R. A., and Forsén, S. (1966) *Prog. NMR Spectrosc. 1*, 15−204.
32. Skelton, N. J., Kördel, J., Akke, M., and Chazin, W. J. (1992) *J. Mol. Biol. 227*, 1100−1117.
33. Hwang, T. L., Mori, S., Shaka, A. J., and Van Zijl, P. C. M. (1997) *J. Am. Chem. Soc. 119*, 6203−6204.
34. Hwang, T. L., Van Zijl, P. C. M., and Mori, S. (1998) *J. Biomol. NMR 11*, 221−226.
35. Kroenke, C. D., Loria, J. P., Lee, L. K., Rance, M., and Palmer, A. G., III (1998) *J. Am. Chem. Soc. 120*, 7905−7915.
36. Tjandra, N., Feller, S. E., Pastor, R. W., and Bax, A. (1995) *J. Am. Chem. Soc. 117*, 12562−12566.
37. Kay, L. E., Torchia, D. A., and Bax, A. (1989) *Biochemistry 28*, 8972−8979.
38. Peng, J. W., and Wagner, G. (1992) *J. Magn. Reson. 98*, 308−332.
39. Davis, D. G., Perlman, M. E., and London, R. E. (1994) *J. Magn. Reson., Ser. B 104*, 266−275.
40. Mandel, M. A., Akke, M., and Palmer, A. G., III (1996) *Biochemistry 35*, 16009−16023.
41. Luz, Z., and Meiboom, S. (1963) *J. Chem. Phys. 39*, 370.
42. Halle, B., and Wennerström, H. (1981) *J. Chem. Phys. 75*, 1928−1943.
43. Lipari, G., and Szabo, A. (1982) *J. Am. Chem. Soc. 104*, 4559−4570.
44. Lipari, G., and Szabo, A. (1982) *J. Am. Chem. Soc. 104*, 4546−4559.
45. Fast, J., Hakansson, M., Muranyi, A., Gippert, G. P., Thulin, E., Evenas, J., Svensson, L. A., and Linse, S. (2001) *Biochemistry 40*, 9887−9895.

BI015945N